2-D MODELLING OF RIVER ICE THERMAL MELTING

by

S.Sarraf[1], P. R. Plouffe[2], and R. Kahawita[3]

ABSTRACT

Thermal effluent is discharged by municipalities, industries and thermal power plants into nearby streams. Where rivers are ice covered for a longe period of the year, these thermal effluents have the effect of melting the ice cover over long reaches. Ice cover melting is primarily function of the the prevailing meteorological conditions, the hydrodynamic characteristics of the receiving stream, and the effluent source magnitude.

A two-dimensional numerical model for the melting of river ice cover is developed. The flow field is simulated by solution of the St. Venant equations incorporating the effect of the ice cover on the flow. Temperature distribution is modelled by the use of the unsteady two-dimensional energy transport equation. Ice thickness is simulated by use of the atmospheric heat exchange processes and heat transfer from the river flow to the ice cover. The model is applied for a number of test cases and compared to an analytical solution. Comparison is also carried out with a set of field data on the Mississippi River near Bettendorf, Iowa.

1) Assistant Professor, Department of Civil Engineering, Concordia University , 1455 De Maisonneuve Blvd. W., Montréal, Québec, CANADA, H3G 1M8, Tel: (514) 848-7811

INTRODUCTION

Throughout the world large amounts of waste heat are being rejected to nearby watercourses from thermal power plants, industries and municipalities. In cold regions where rivers are ice covered for part of the year, these effluents have the effect of partially melting the ice cover, reducing its thickness, or completely suppressing its formation over long reaches. Ice cover melting is primarily function of the the prevailing meteorological conditions, the hydrodynamic characteristics of the receiving stream, and the effluent source magnitude.

Dingman et al. (1967) performed a one-dimensional solution of the energy equation neglecting the diffusion term. A steady state solution was calculated using a uniform, assumed velocity field. Paily (1974) solved the one-dimensional energy equation including the effect of longitudinal dispersion. Ashton (1979) solved the one-dimensional quasi-steady energy equation. Heat transfer processes at the ice cover interfaces were considered as well as varying meteorological conditions, using a linear heat transfer relation. An assumed uniform and steady velocity field was used. Shen and Chiang (1984) developed a one-dimensional model of the ice cover growth and decay on the St. Lawrence River. The model used an uniform velocity field and included a complete ice cover and open water heat transfer formulation. Sarraf & Salah (1987) performed an analytical solution of the one-dimensional energy equation, including coverging or diverging river flow. A linear heat transfer relation was used in the solution.

In the present work, river ice cover melting by a thermal effluent is modelled by a two-dimensional numerical model. The unsteady two-dimensional energy equation is used for the water temperature calculation. Heat transfer processes between the river and the atmosphere is incorporated both for the open water and ice covered cases.

MATHEMATICAL FORMULATION

Hydrodynamic Equations

The flow field is calculated using the depth averaged shallow water equations. These equations are expressed in conservative form as follows:

- Continuity Equation:

$$\frac{\partial H}{\partial t} + \frac{\partial U}{\partial x} + \frac{\partial V}{\partial y} = 0 \qquad (1)$$

- Momentum Conservation (x direction):

$$\frac{\partial U}{\partial t} + \frac{\partial E}{\partial x} + \frac{\partial F}{\partial y} = gh(S_{ox} - S_{fx}) + fV - \frac{1}{\rho}\tau_{sx} + \frac{\partial}{\partial x}(\varepsilon h \frac{\partial u}{\partial x}) + \frac{\partial}{\partial y}(\varepsilon h \frac{\partial u}{\partial y}) \qquad (2)$$

- Momentum Conservation (y direction):

$$\frac{\partial V}{\partial t} + \frac{\partial F}{\partial x} + \frac{\partial G}{\partial y} = gh(S_{oy} - S_{fy}) - fU - \frac{1}{\rho}\tau_{sy} + \frac{\partial}{\partial x}(\varepsilon h \frac{\partial v}{\partial x}) + \frac{\partial}{\partial y}(\varepsilon h \frac{\partial v}{\partial y}) \qquad (3)$$

where x and y the horizontal coordinates; t the time; H=H(x,y,t) the water surface elevation;

h=h(x,y,t) the local water depth; U=U(x,y,t) =uh and V=V(x,y,t)=vh the unit width discharges in x and y directions respectively; E, F, and G are defined as:

$$E = E(x,y,t) = u^2h + 1/2\ g(h + 0.9\theta)^2 \quad (4)$$

$$F = F(x,y,t) = uvh \quad (5)$$

$$G = G(x,y,t) = v^2h + 1/2\ g(h + 0.9\theta)^2 \quad (6)$$

S_{ox} and S_{oy} are the river bed slopes; S_{fx} and S_{fy} are the friction slopes; g the gravitational acceleration value; R the hydraulic radius; f the Coriolis parameter; τ_{sx} and τ_{sy} the surface stresses respectiveely developed by wind action; ε the turbulent viscosity coefficient and ρ the water density. The additional pressure due to the weight of the ice cover is accounted for by adding 90% of the ice thickness θ to the water depth in hydrostatic pressure terms.

Energy Equation

The temperature distribution in the flow is determined from the two dimensional temperature equation:

$$\frac{\partial Th}{\partial t} + \frac{\partial TU}{\partial x} + \frac{\partial TV}{\partial y} = \frac{\partial}{\partial x}\left(hD_x \frac{\partial T}{\partial x}\right) + \frac{\partial}{\partial y}\left(hD_y \frac{\partial T}{\partial y}\right) + \Phi \quad (7)$$

where D_x is the heat diffusion term in the x direction; D_y is the heat diffusion term in the y direction; T is the water temperature and Φ is the source term. The source term is calculated from equation (8) where ϕ_S is the heat added to the water from the atmosphere and the ice cover and C_p is the specific heat of water [Paily ,1974]:

$$\Phi = \frac{\phi_S}{\rho C_p} \quad (8)$$

The solution of the energy equation requires the evaluation of the dispersion coefficient terms D_x and D_y. These terms are determined from the following equations [Ashton 1979]:

$$D_x = k_x\ U^*R \quad (9)$$

$$D_y = k_y\ V^*R \quad (10)$$

where k_x is the longitudinal dispersion constant in the x direction; k_y is the longitudinal dispersion constant in the y direction; U* is the shear velocity in the longitudinal direction and V* is the shear velocity in the transverse direction.

Engman (1977) found that the presence of an ice cover reduces the dispersion constants by 50%. However, by the use of the hydraulic radius, which is reduced by one half in the case of an ice covered river, one value may be used for the dispersion constant. In field situations, the dispersion constant is influenced by wind, waves, and channel irregularities. In rivers a large variation in the dispersion constant is measured, with much larger values being reported. The coefficient constant in both x and y directions used in this work was set to 10.

Surface Heat Exchanges

For a free ice stream, heat exchange with the atmosphere occurs at the air-water interface while for an ice covered stream this occurs at the air-ice interface. The components of the heat exchange include shortwave (solar) radiation, longwave radiation, evapo- condensation flux and conductive heat transfer. The meteorological factors determining these components are cloud cover, air temperature, wind velocity and air vapour pressure. Heat transfer from precipitation and geothermal heat transfer through the river bed is not significant in modelling the melting of river ice by thermal effluent. Due to the that the ice edge is normally washed free of snow by wave action, the effect of snow cover is not being considered in this work. The heat transfer processes are outlined in Fig. 1.

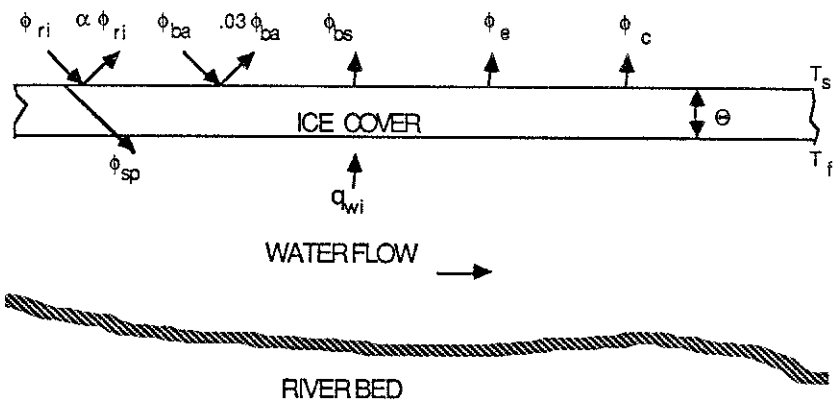

Fig. 1. Heat transfer processes through stream ice cover.

When ice is not present, this heat transfer occurs directly between the air and the water. The heat transfer involves several components which are dependent on the air temperature, surface temperature, wind velocity, solar and atmospheric radiation, and the humidity. If ice is present, the only direct heat transfer to the water is from the solar radiation which penetrates the ice cover. The ice surface temperature is calculated from the heat exchange processes, assuming a linear temperature distribution over the ice cover, with the bottom surface at the freezing point.

- Equation of Ice Cover Evolution

River ice cover consists of a floating slab with heat transfer and thickness changes occurring at both the top and bottom surfaces. The top surface exchanges heat with the atmosphere and at the bottom surface heat exchange occurs with the river flow. The top surface of the floating ice cover is assumed to be well drained and thickening of the ice cover is solely occurring at the bottom surface. Within the ice cover, heat transfer is governed by one-

dimensional heat conduction and the temperature profile is assumed to be linear. Top surface temperature is determined from meteorological conditions. Bottom surface temperature at the water-ice interface is set to the freezing point temperature. Top surface temperature of the ice cover is determined by the heat exchanges occurring at the air-ice interface. In order to calculate the surface temperature, each of the above top surface heat exchange process is evaluated and substituted in the following equation:

$$\phi_S (1 - \beta_i e^{-\tau_i \theta}) - \phi_b - \phi_e - \phi_c + K_i \frac{T_f - T_s}{\theta} = 0 \qquad (11)$$

where K_i is the thermal conductivity of ice. The thermal conductivity of ice is 0.53 cal m^{-1} $s^{-1}°C^{-1}$.

The top surface melting can be calculated using:

$$\phi_S(1 - \beta_i e^{-\tau_i \theta}) - \phi_b - \phi_e - \phi_c + K_i \frac{T_f - T_s}{\theta} = - \rho_i L_i \frac{\Delta\theta_s}{\Delta t} \qquad (12)$$

where ρ_i is the density of ice; L_i is the latent heat of fusion of ice and $\Delta\theta_s$ is the change in the ice thickness at the upper surface during the time step Δt. The density of ice is 920 kg m^{-3} and the heat of fusion of ice is 8.0×10^4 cal kg^{-1} [Shen & Chiang 1984].

At the bottom surface of the ice cover, water provoke melting or growth of the ice cover, depending on the ice cover heat exchanges. The ice cover thickness change at bottom face can be determined from [Ashton, 1979]:

$$K_i \frac{T_f - T_s}{\theta} - q_{wi} = \rho_i L_i \frac{\Delta\theta_w}{\Delta t} \qquad (13)$$

where $\Delta\theta_w$ is the change in the ice thickness at the water interface during the time step Δt. q_{wi} (cal m^{-2} s^{-1}) is the turbulent heat transfer from the water to the ice cover given by:

$$q_{wi} = h_{wi} (T - T_f) \qquad (14)$$

where the heat transfer coefficient h_{wi} is determined with anology to a closed conduit flow and given by :

$$h_{wi} = C_{wi} \frac{V^{0.8}}{h^{0.2}} \qquad (15)$$

where h_{wi} is the heat transfer coefficient water to ice in cal m^{-2} s^{-1} $°C^{-1}$, V is the resultant velocity in ms^{-1} and C_{wi} is the heat transfer constant. The value of C_{wi} is 387.4 cal $s^{-0.2}$ $m^{-2.6}$ $°C^{-1}$.

NUMERICAL FORMULATION

Solution of the hydrodynamic equations utilizes a modified McCormack finite difference scheme [Baldwin et al. 1975]. The modified McCormack scheme is an explicit, forward time central space scheme. The scheme is a fractional step method involving the division of a finite

difference operator into a sequence of simpler steps. The two-dimensional operator is split into a sequence of one-dimensional operators. Each operator is further split into a predictor-corrector sequence. The L_x operator calculates the derivatives in x-direction and the L_y operator calculates the derivatives in y-direction. The modified McCormack scheme splits both the x and y derivatives into two time steps, each one half of the original time step. By splitting both x and y derivatives, as opposed to the original scheme where only one direction was split, no preferred alignment in the flow direction of the scheme is necessary. The modified McCormack scheme uses the series of operators:

$$[L_x \quad Ly \quad L'_y \quad L'_x] \tag{16}$$

where in the operators L_x and L_y, backward differences are used in the predictor step and forward differences are used in the corrector step. In the L'_x and L'_y operators, forward differences are used in the predictor step and backward differences are used in the corrector step. The use of a symmetric sequence allows for second order accuracy in space and time.

An upwinding finite difference scheme is used to appoximate the energy equation [Roache 1976]. The upwind scheme is an explicit forward time method. This scheme takes into account the direction of the convecting velocity. In cases where convective heat transfer dominates dispersive heat transfer, central difference schemes do not give usable results. The cell wall dispersion coefficient is determined by use of the harmonic mean of the adjacent cell values [Patankar 1980].

MODEL APPLICATIONS AND DISCUSSIONS

The model developed in this work has been used for a number of situations to illustrate the behaviour of the river ice cover near the source of a thermal effluent. At first a simple rectangular channel geometry has been chosen for these tests. The channel has a flat bed, a water depth of 3 m, and a constant width of 750 m . The flow enters the channel at the left and flows to the right with a velocity of 0.2 m s^{-1}. The Manning roughness coefficient for the channel bed is taken as 0.030 while for the ice cover underside as 0.020. The coefficient of turbulent viscosity is 0.25 m^2s^{-1}. A value of 10.0 is used for the dispersion constants. A side thermal effluent discharges into the channel with a flow rate of 4.5 m^3s^{-1}. Initial ice thickness is set to 0.10 m. A grid spacing of 500 m in the x direction and 50 m in the y direction are used with a time step of 15.0s. The prevalent meteorological conditions are : cloud cover = 5 tenths, wind velocity = 20 km/h, relative humidity = 60%, and air temperature varies from -5 to -30°C.

The transverse ice thickness at the outfall and the mid-reach sections is shown in Fig. 2 and 3 for an air temperature of -20° C and an effluent temperature of 10°C for three different velocity conditions. The transverse velocity profiles at the above mentioned sections are shown on Fig. 4. Near the shores some reduction in velocity occursdue to the non-slip boundary condition employed, however, the ice cover melting causes an increase in the flow velocity of 25% as compared to the other shore. The mid-reach section, where ice thickness is reduced,

shows a 5% velocity increase between shores. A check of inflow and outflow quantities shows an agreement within 1.5% of the flow.

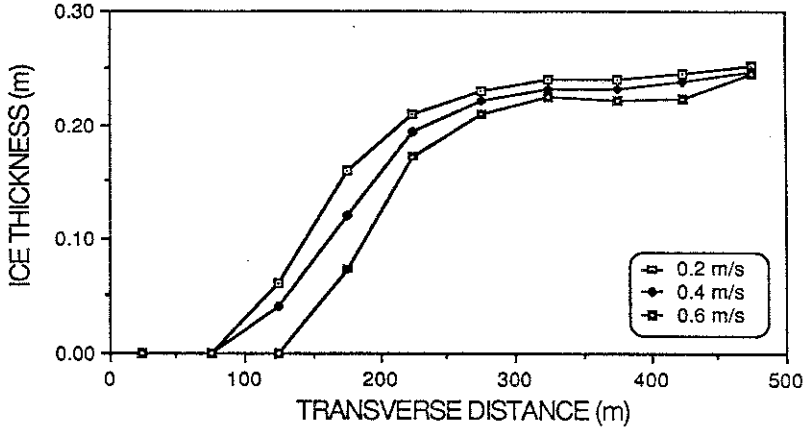

Fig. 2 Ice Thickness Profile at 500 m Below Effluent Source.

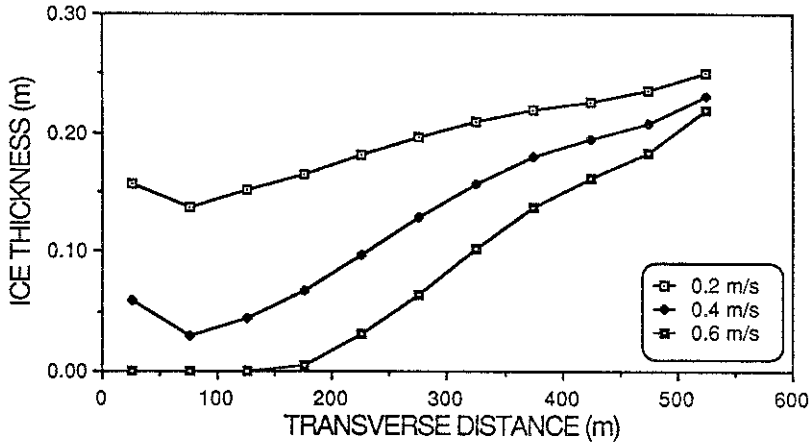

Fig. 3 Ice Thickness Profile at Channel Mid-Reach.

The ice thickness distribution field shown in fig 4 illustrates in contour line form the magnitude of the ice free reach due to the thermal effluent effects. The ice melting occurs predominately downstream, near the shore, on the side of the effluent discharge. A slight reduction in ice thickness occurs upstream of the point of discharge over a distance of 500 m. In the transverse direction the ice cover quickly thickens to the undisturbed thickness over a distance of about 150 m, as one moves across the channel from the effluent source. The ice cover thickens much more slowly in the longitudinal direction over a distance of 10 km, downstream of the ice

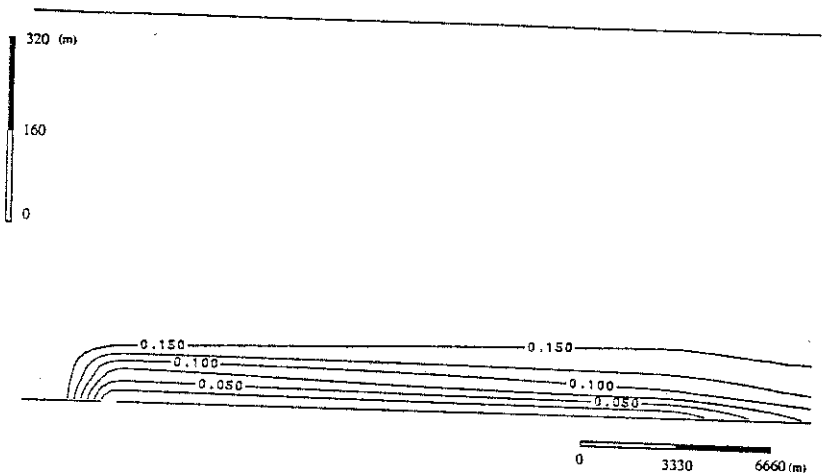

Fig. 4 Contour Line of Ice Thickness Distribution Field.

free reach. This is caused by a lower temperature gradient than in the transverse direction. In the case of low air temperature and a low effluent discharge temperature no ice free region occurs, only a reduction in thickness.

- Field Case Computations

In February 1980 the U.S. Army Cold Regions Research and Engineering Laboratory carried out a field study on the melting of river ice by a side discharge thermal effluent. The study was performed on the Mississippi River near Bettendorf, Iowa. At the site, the Mississippi River is approximately 1 km in width, narrowing in the downstream direction. The discharge during the study period was almost constant at 850 m^3s^{-1}. The water depth varies from 2 m near the shore to a maximum of 10 m in the main channel. Average velocity of the flow is 0.25 $m\ s^{-1}$. The river bed consists of sandy clay material with no rocks and few sudden changes in elevation. A Manning coefficient of 0.030 is used to represent the bed roughness.

The geometry of the river valley looking upstream from the outflow boundary can be depicted from Fig. 5 which also shows the calculated velocity field. The side discharge thermal effluent originates from the Riverside thermal power plant. The thermal discharge characteristics were determined from plant operating records. During the study period the daily average discharge was almost constant with a mixed temperature of 2.97°C.

A complete meteorological record of 3 hour readings is available from the Moline, Illinois airport weather office located 6 miles from the study site. Air temperature, wind velocity, humidity, cloud cover and precipitation records are given. During the study period, from

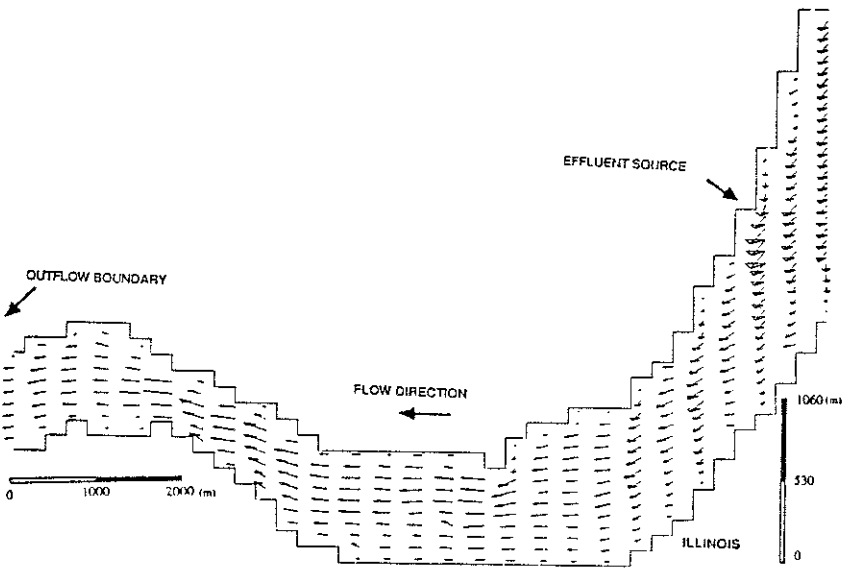

Fig. 5 Computed Velocity Field for Mississippi River, February 14.

February 14 to February 17 the air temperature was initially warm and then became cold. The meteorological variables for the dates of February 14 and February 17 are summarized in Table 1.Temperature readings of the water were taken at a few locations during the field study. These readings indicated a constant variation of temperature with depth, indicating complete mixing in the vertical direction. At the entrance to the study reach, an inflow water temperature of slightly above 0°C was found. The value of 0.05°C is used for the inflow water temperature in the model. A value of 10.0 is used for the dispersion constants, due to the gentle flow of the river.

Table 1 Field Study Meteorological Conditions

Parameter & unit	February 14	February 17
Air temperature °C	- 2.13	-18.75
Cloud Cover tenths	9.8	0.0
Latitude degrees	41.5	41.5
Wind Velocity m s^{-1}	4.20	3.99
Vapour Pressure mb	2.10	1.05

Ice cover edge locations were determined from oblique aerial photographs, taken during overflights of the river. The cold weather during the study period caused a reduction in the length of the open water reach. A thin ice covering formed over previously open water on February 17. The ice cover underside was relatively smooth with a few ripples. A Manning coefficient of 0.020 was used in the model for the ice cover underside. Snow accumulation on the river ice cover was negligible. No significant amounts of frazil ice was present in the river flow, due to a complete ice cover upstream of the study reach. A grid spacing of 125 m in the x-direction, 25 m in the y-direction and a time step of 4.5 s is used in the calculations.

The computed velocity field for the ice cover condition on February 14 is shown in Fig. 5. On Fig. 6 and on Fig. 7 the model temperature and ice thickness distributions of the river respectively. As seen in Table 2 the model correctly predicts whether suppression of the river ice will occur. The length of the downstream reach calculated by model especially on February 14, compares well with the field study findings. Much of the difference in the findings may be a result of a number of small thermal effluent discharges not accounted for in the field study data and therefore not included in the model calculations. These discharges would have the effect of lengthening the ice free reach.

Table 2 Comparison of Ice Free Reaches

	February 14		February 17	
	Field Study	Model	Field Study	Model
Ice Free Reach	yes	yes	yes	yes
Downstream Length km	8.0	6.6	4.3	1.9

On Februay 17 a much greater undisturbed ice thickness is present on the channel, following the cold weather period. A greater ice thickness was present in bays with low flow velocity. Furthermore a small area of thin ice is present on the shoreline on the side of the effluent discharge.

A comparison of the field study findings and model results is given in figures 8, and 10. In Fig.10 the model correctly predicts whether suppression of the river ice does occur. The length of the downstream reach calculated by model especially on February 14, compares well with the field study measurement. The slight discrepancy with the in the field findings for February 17 may be attributed to a number of small thermal effluent discharges whose magnitudes are not available and therefore not be accounted for in the model calculations. The presence of these discharges would have the effect of lengthening the ice free reach. The two most significant of these side discharges is located approximately 1.5 km downstream of the power plant.

Fig. 8 shows a comparison of the river flow temperature at the mid-point of the ice free reach for February 17. The mid-depth temperature readings are used. Good agreement initially

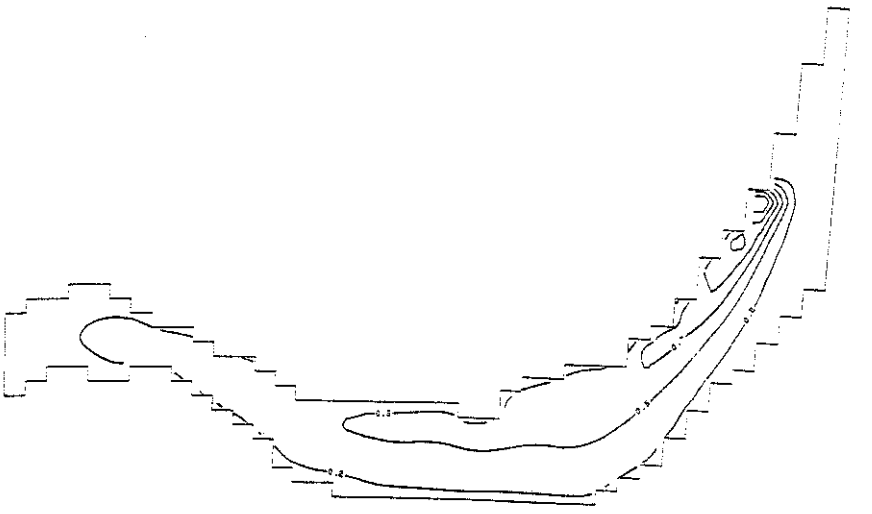

Fig. 6 Computed Temperature Distributions for Mississippi River, February, 17.

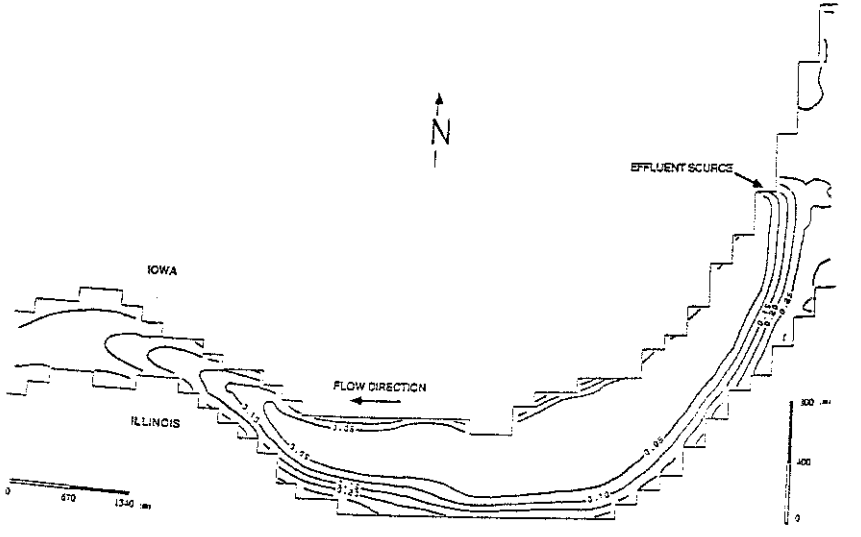

Fig. 7 Ice Thickness Distributions for Mississippi River, February, 14.

occurs within 2% but then some divergence of up to 30%, again likely caused by the minor effluent sources. No field water temperature data is available for February 14.

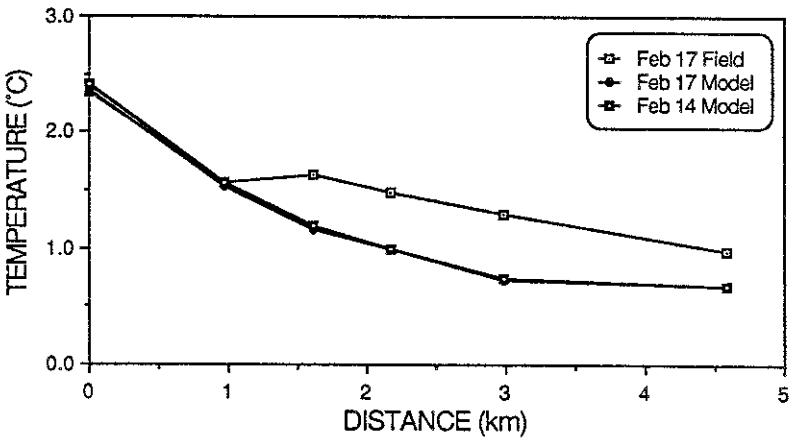

Fig. 8 Longitudinal Temperature Comparison.

Fig. 9 shows a comparison of transverse section temperature profiles for February 17. The comparison is for the width of the ice free reach from the shore. The maximum water temperature occurs a short distance from the shore. The discrepancy at the downstream section is again likely causaed by the minor effluent sources. Fig. 10 shows a comparison between the ice free width predicted and measured on Feburary 17 with agreement within 12%. The ice thickness for several x-direction sections are shown on Fig. 11 for February 14, again with less sharp profiles downstream.

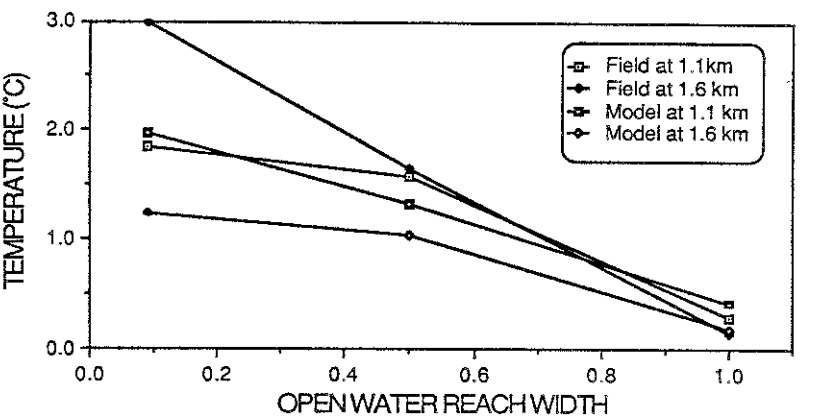

Fig. 9 Transverse Temperature Comparison - February 17.

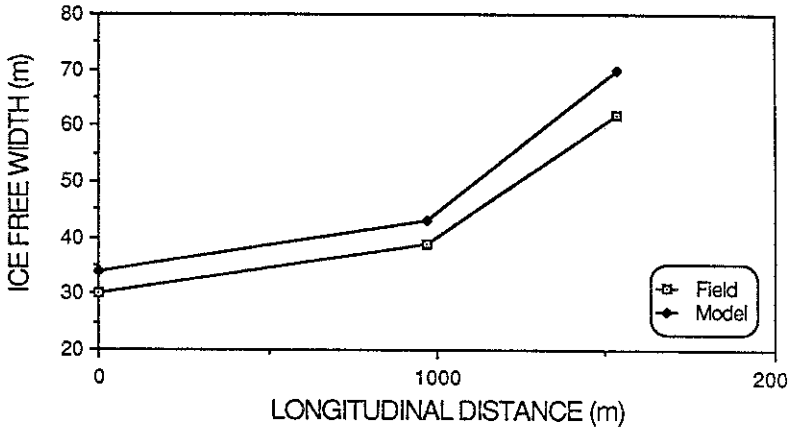

Fig. 10 Ice Free Width Comparison.

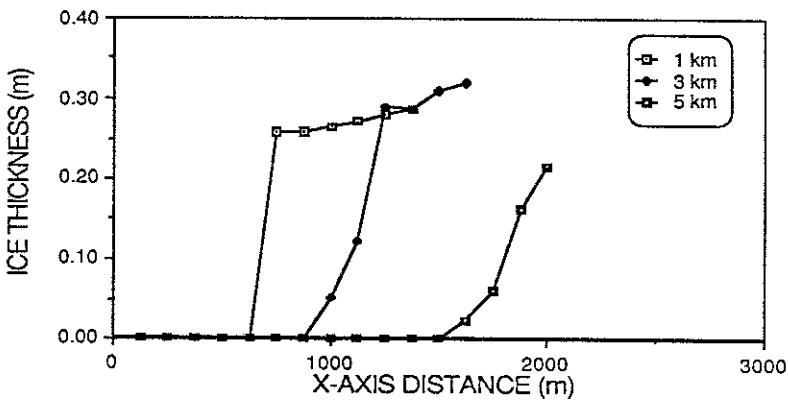

Fig. 11 Ice Thickness Profiles.

CONCLUSIONS

In the present work the melting of river ice by a side discharge thermal effluent is modelled. The river hydrodynamics are simulated by use of the shallow water equations. An extensive heat budget evaluation allows for the effect of different meteorological conditions to be considered. Tests indicated that warmer effluent discharges increased open water reaches in length and width. The ice cover thickens quickly in the direction transverse to the flow but thickens slowly in the main flow direction, due to a lower water temperature gradient.

The McCormack finite difference scheme produces a good simulation of the flow field. Temperature distribution modelling is performed by use of an upwinding finite difference scheme, due to the inability of central difference schemes to provide useful results. A comparison

with an analytical solution of the energy equation is carried out indicating overall good performance of the model. Simulation of a real life case shows the validity of the behaviour of the ice cover simulation. The space distribution of ice cover thickness distribution agrees with the field results.

ACKNOWLEDGEMENTS

This work was partially supported by FCAR-EQ-3016 (Québec) and NSERC-A-4899 grants which are gratefully acknowledged. The author wish to thank Dr. George Ashton (US-CRREL) for his assistance in providing the field data.

REFERENCES

Ashton, G.D. (1979), "Suppression of River Ice by Thermal Effluents," CRREL Report 79-30, U.S. Army Cold Regions Research Engineering Laboratory, Hanover, N.H.

Baldwin, B.S., R.W. MacCormack, & G.S. Diewart, (1975), "Numerical Techniques for the Solution of the Compressible Navier-Stokes Equations and Implementation of Turbulence Models", AGARD Lecture Series No. 73, NATO, London, Eng. Feb. pp. 2.1-2.22

Burrell, B. and Davar, K.S. (1982). "Flow Conveyance With Ice Cover on the Nashwaak River, N.B.," Canadian Journal of Civil Engineering, 9, pp. 674-677.

Dingman, S.L., Weeks, W.F. and Yen, Y.C. (1967). "The Effects of Thermal Pollution on River Ice Conditions, Part 1, A General Method of Calculation," CRREL Report 206, U.S. Army Cold Regions Research Engineering Laboratory, Hanover, N.H.

Engman, E.O. (1977). "Turbulant Diffusion in Channels with a Surface Cover," Journal of Hydraulic Research, 15 (4) , pp. 327-335.

Paily, P.P. (1974). "Winter-Regime Thermal Response of Heated Streams," Ph.D. Thesis, University of Iowa.

Patankar, S.V. (1980). Numerical Heat Transfer and Fluid Flow, Hemisphere Publishing Company, Washington, D.C.

Roache, P.J. (1976). Computational Fluid Dynamics, Hermosa Publishers, Alburquerque, N.M.

Sarraf, S., and Saleh, W., (1987), " Local Melting of Ice Cover by Thermal Side Effluent", ASCE J. Cold Regions Engineering, Vol. 1, No. 3, pp 105-121.

Shen, T.S. and Chiang, L. (1984). "Simulation of Growth and Decay of River Ice Cover", Journal of Hydraulic Engineering, ASCE, 110, (7), pp. 958-971.

NOTATION

C_p	specific heat of water, in cal kg^{-1} $°C^{-1}$
D_x, D_y	dispersion coefficients in x and y directions, in m^2 s^{-1}
e_a	air vapour pressure, in mb
e_s	saturation vapour pressure, in mb
g	gravitational acceleration, in m s^-
H	water surface elevation, in m
h	water depth, in m
h_{wi}	heat transfer coefficient from water to ice cover, in cal m^{-2} s^{-1} $°C^{-1}$
K_i	ice thermal conductivity, in cal $m^{-1}s^{-1}$ $°C^{-1}$
k_x, k_y	dispersion constant x and y directions direction
L_i	ice heat of fusion, in cal kg^{-1}
n	composite Manning coefficient
n_b	Manning coefficient of river bed
n_i	Manning coefficient of underside of ice cover
R	hydraulic radius, in m
T	water temperature, in °C

T_a	air temperature, in °C
T_s	top surface temperature, in °C
t	time, in sec.
u, v	flow velocity in x, and y directions, in m s^{-1}
V_a	wind velocity at 2 m above surface, in m s^{-1}
x, y	space coordinate , in m
Z_f	bed elevation, in m
ε	turbulant viscosity coefficient, in m^2 s^{-1}
θ	ice thickness, in m
ρ	water density, in kg m^{-3}
ρ_i	ice density, in kg m^{-3}
σ	Stefan-Boltzman constant, in cal cm^{-2} day^{-1}
Φ	source term, in °C s^{-1}
ϕ	heat transfer to water, in cal cm^{-2} day^{-1}
ϕ_{ba}	atmospheric radiation, in cal cm^{-2} day^{-1}
ϕ_c	conductive heat transfer, in cal cm^{-2} day^{-1}
ϕ_e	evapo-condensation flux, in cal $cm^{-2}day^{-1}$
ϕ_{ri}	incoming shortwave radiation, in cal cm^{-2} day^{-1}

5th Ice Workshop

Discussion Form

PAPER: 2-D Modelling of River Ice Thermal Melting
AUTHOR: P.R. Plouffe, S. Sarraf
QUESTION BY: T.D. Prowse

QUESTION/COMMENT:
Have you considered the use of water to ice heat transfer coefficients which directly incorporate an ice roughness term? Field experiments of the heat flux to intact and fragmented ice show that they provide better results than those, such as the one used in the paper from Hayes and Ashton (1985), which don't consider roughness.

Response:

The present numerical model differs from Hayes and Ashton(1984) work by the fact that this is not only a thermal transport model but also a hydrodynamic model as well. Thus, employing a special heat transfer coefficient may not be needed since the effects of ice induced shear stress are accounted for in the hydrodynamic equations and consequently reflected in the thermal balance conditions. However, in the near future, we will experiment the use of such coefficients, report the results to Dr Prowse and certainly publish the findings.

5th Ice Workshop

Discussion Form

PAPER: 2-D Modelling of River Ice Thermal Melting
AUTHOR: Sarraf et al
QUESTION BY: Doug Hodgins, MacLaren Plansearch

QUESTION/COMMENT:
It appears from Figure 5 that you are introducing an average, unmonitored velocity across your upstream boundary. Your effluent source is in the fourth column of your array, where it appears that boundary conditions are still influencing the hydrodynamics.

Could this be affecting the results of Figures 8 and 9, and would you expect different results if you had begun modelling ≈ 2000 m further upstream? You may not have perfect bathymetric data, but it would be of value to use navigational charts in these simulations before you test further parameter adjustments.

Response:

I completely agree with the remark of Mr. Hodgins concerning the effect of the upstream boundary conditions. A new configuration of the mesh has been implemented with the calculation starting about 1.5 km upstream. On the other hand, the effluent was positioned at the 9^{th} grid cell and not at the fourth as may be deduced form fig 8 and 9. Also, the bathymetry is of higher resolution than the grid spacing and therefore no improvement can be done unless the grid is further refined.